A continuum damage relation for hydrogen attack cavitation

van der Burg, M.W.D.; van der Giessen, E.

Published in:
Acta Materialia

DOI:
10.1016/S1359-6454(96)00382-5

Publication date:
1997

Pergamon

PII: S1359-6454(96)00382-5

Acta mater. Vol. 45, No. 7, pp. 3047–3057, 1997

Published by Elsevier Science Ltd

1359-6454/97 $17.00 + 0.00

A CONTINUUM DAMAGE RELATION FOR HYDROGEN ATTACK CAVITATION

M. W. D. VAN DER BURG and E. VAN DER GIESSEN

Delft University of Technology, Laboratory for Engineering Mechanics, P.O. Box 5033, 2600 GA Delft, The Netherlands

(Received 2 August 1996)

Abstract—A continuum damage relation (CDR) is proposed to describe the failure process of hydrogen attack, i.e. grain boundary cavitation of steels under conditions of high temperature and high hydrogen pressure. The cavitation is caused by the chemical reaction of hydrogen with grain boundary carbides forming cavities filled with high pressure methane. The micromechanisms described are the grain boundary cavitation and the dislocation creep of the grains. The CDR is based on two extreme cavitation rate distribution modes. In the first mode, the cavitation rate along the facets is uniform, resulting in a hydrostatic dilatation while the creep deformations remain relatively small. In the second mode, cavitation proceeds predominantly on grain boundary facets transverse to the principal macroscopic stress. This part of the CDR builds on Tvergaard's constituitive relation for intergranular creep rupture [Tvergaard, V., *Acta metallurgica*, 1984, **32**, 1977] where the facet cavitation is constrained by creep of the surrounding grains. The mode corresponding to the highest cavitation rate is the active mode. The two-dimensional version of the CDR is verified against detailed finite element analyses of hydrogen attack in planar polycrystalline aggregates. Finally, the generalization to a three-dimensional CDR is discussed. © *1997 Acta Metallurgica Inc.*

1. INTRODUCTION

Many processes in the petrochemical industry are performed at high temperatures in a hydrogen rich environment. Under these circumstances, the lifetime of high pressure vessels is determined by hydrogen attack (HA) corrosion [1]. HA is the cavitation of grain boundary facets which is believed to occur as follows [2, 3]. Dissolved hydrogen in the steel reacts with a grain boundary carbide forming methane gas. Contrary to the hydrogen, the methane molecule cannot diffuse away through the steel, so subsequently a methane filled cavity originates at the carbide. The cavitation is driven by the pressure inside the cavity, but can be accelerated significantly by macroscopically applied stresses. Depending on the reactivity of the carbide, the methane pressures can be of the order of the remote macroscopic stresses, though in the case of aggressive carbide, orders of magnitude larger [4]. Driven by the pressure and/or applied stresses, the cavities grow by grain boundary diffusion in combination with dislocation creep in the adjacent grains. When the cavities on the grain boundary facets have grown so large that they coalesce, a microcrack occurs. Linking-up of these microcracks results in a macroscopic intergranular fracture.

The HA cavitation process can be investigated on three length scales, each differing by an order of magnitude. Initial investigations were at the cavity-size length scale, and focused on the growth of a single cavity under a constant stress state [2–6]. The interaction between grain boundary diffusion and dislocation creep was shown to be sensitive to the stress triaxiality. The results for high stress triaxialities especially are of interest because these stress states are present during HA. The volumetric growth rates determined by the detailed numerical analyses could be captured fairly well by an analytical growth rate relation [6]. Using this cavity growth relation, the damage evolution could be established and first estimates of lifetimes could be made [4]. However, as is well known for creep rupture, the cavitation evolution can be influenced significantly by the deformations of the surrounding grains. This was investigated in Ref. [7] at the second, grain-size length scale, where the HA evolution was analysed in polycrystalline aggregates. Nonuniform carbide distributions along the grain boundaries were the subject of analysis since in real material carbides are also nonuniformly distributed. The results of the numerical analyses demonstrated the development of internal stresses, influencing the cavitation rate along the grain boundary facets. Depending on material parameters, the times to cavity coalescence in the polycrystal investigations were found to sometimes differ significantly from the first lifetime estimates obtained with the single cavity model. Finally, the third length scale is that of a component in which one is interested in the global HA development. The degree of HA will vary over the specimen due to gradients in, e.g. temperature and/or hydrogen

pressure in the material. For these analyses the polycrystal unit cells used in Ref. [7] are far too small, and to perform a polycrystal unit cell analysis at each integration point of the engineering component FE mesh is too CPU time consuming. Hence, an analytical continuum damage relation describing HA is needed.

In the present paper, a constitutive damage relation describing the evolution of hydrogen attack is proposed. The relation is based on two models which describe the two contrasting modes in which HA cavitation in a polycrystalline aggregate was observed to develop in Ref. [7]. For the so-called dilatant cavitation mode, a new model is introduced, called the rigid grain model, in which (creep) deformations of the grains are neglected. Due to the virtually rigid grains, the cavitation rate along the grain boundaries can only be uniform. For the other (nonuniform) cavitation mode, Tvergaard's continuum damage model for creep failure by grain boundary cavitation [8, 9] is adopted. This model is based on an idea of Rice [10], where creep controlled cavitation is described by matching the opening rate of a facet-size virtual crack in a creeping body with the grain boundary cavitation rate over a grain facet. First, a two-dimensional version of the new constitutive relation for HA damage is formulated for plane strain problems. This CDR is then verified against detailed finite element analyses of HA in planar polycrystalline aggregates, using the cell analysis technique of Ref. [7]. The comparison is made in terms of the evolution of cavitation damage and associated normal stress, as well as the macroscopic principal strains at failure. Attention is confined to applied states of stress in which the direction of the maximal principal tensile stress remains the same during the process. Finally, the three-dimensional generalization of the CDR is discussed.

In this paper, tensors are denoted by bold-face letters. The scalar or double-dot product between two second-order tensors $\mathbf{A}$ and $\mathbf{B}$ is denoted as $\mathbf{A}:\mathbf{B}$, so that $\mathbf{A}:\mathbf{B} = A^{ij}B_{ij}$ with A^{ij} and B_{kl} being their contravariant and covariant components, respectively. The tensor $\mathbf{I}$ is the unit tensor.

2. CAVITY GROWTH DUE TO HA

On our smallest length scale, we deal with the growth of a single cavity. In the model cavities only nucleate from carbides present from the beginning, according to observations for 2.25Cr–1Mo steels [11]. It is assumed that the grain boundary carbides are equal and uniformly distributed along the grain boundary facets. The implications of possible nonuniform distributions of carbides are reported in Ref. [7]. Grain boundary cavitation has been modelled by a cylindrical unit cell containing a central grain boundary cavity [6], which is called the single cavity model. The growth rate of the cavity is a function of the creep and diffusion rate, the stress rate and its current size. The stress state, driving the cavity evolution, consists of the internal cavity pressure and of stresses remote from the cavity.

The internal pressure is due to a mixture of methane and hydrogen gas in the cavity which is due to the reaction of hydrogen, diffused into the material, with carbides present in the steel to form methane. Methane cannot diffuse away so a cavity originates at the carbide location. The pressure inside the cavity p_m consists of the partial equilibrium methane pressure p_{CH_4} and the partial hydrogen pressure p_{H_2}. The total pressure in this non-ideal gas mixture, p_m, is approximately given by [4]

$$p_m = p_{CH_4} + p_{H_2}.$$

Due to this internal pressure the cavities develop. The most dangerous locations for cavitation are the grain boundaries, not only because most carbides are located there, but also because small cavities located there can grow rapidly by grain boundary diffusion. Since the grain boundary carbides are most important, these are the only carbides taken into account in the analysis.

The assumption is made that the methane pressure is constant in the cavity during growth. Shih and Johnson [5] showed that during cavity growth, the equilibrium methane pressure is not reached in certain cases. As a result, the evolution rate in the model is sometimes overestimated, resulting in a conservative lifetime prediction.

The geometry of a spherical-caps shaped cavity is characterized by its radius a and tip angle ψ (see Fig. 1). The spacing between neighbouring cavities is $2b$. The volume of a cavity V is given by $V = \frac{4}{3}\pi a^3 h(\psi)$, where the geometric parameter $h(\psi)$ is defined as $h(\psi) = [(1 + \cos\psi)^{-1} - \frac{1}{2}\cos\psi]/\sin\psi$.

At elevated temperatures such as encountered in HA situations, the cavities can grow by grain boundary diffusion in combination with dislocation creep in the adjacent grains. By exploiting the insensitivity of the creep and diffusion process on hydrostatic stress the cavity growth problem can be reformulated, as demonstrated in Ref. [6]. A hydrostatic stress p of the magnitude of the internal cavity pressure p_m is superposed on the applied stress state $\boldsymbol{\sigma}'$ (see Fig. 2). Thus, the problem reduces to that

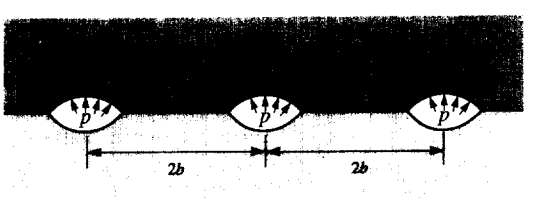

Fig. 1. Spherical-caps shaped cavities on a grain boundary facet with tip angle ψ. The radius of the cavity is a, the spacing between the cavities is $2b$.

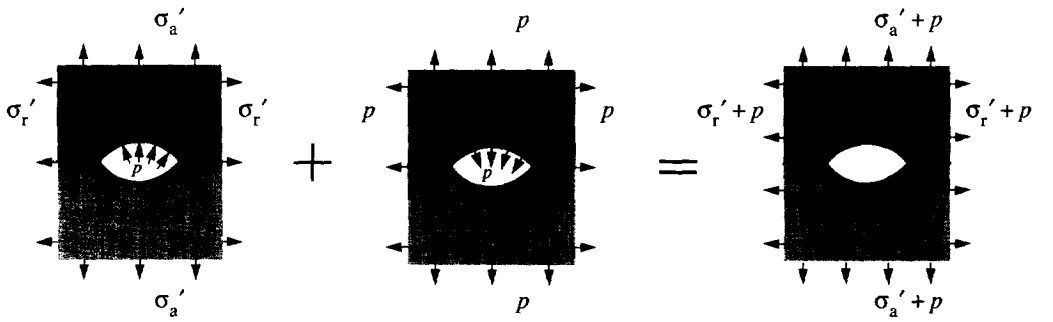

Fig. 2. Superposition of a hydrostatic stress p state to a HA stress situation (σ_a', σ_r'), resulting in a traction free cavity and remote stresses($\sigma_a' + p$, $\sigma_r' + p$).

of a stress-free cavity subjected to a remote stress state of

$$\boldsymbol{\sigma} = \boldsymbol{\sigma}' + p_m \mathbf{I}.$$

The detailed numerical analyses of cavity growth in the cylindrical unit cell have been captured by approximate, yet accurate analytical relations [6, 12, 13] which we will use in the sequel. Here, only a summary of the cavity growth relations is given; the relations are described elaborately in Refs [6] and [4]. The cavity growth rate $\dot{V}$ can be split up into a part based on diffusive cavity growth $\dot{V}_{diff}$ and a part of cavity growth by the dislocation creep $\dot{V}_{cr}$. The total volumetric growth rate is $\dot{V} = \dot{V}_{diff} + \dot{V}_{cr}$. The dependence of the growth rate on the stress state $\boldsymbol{\sigma}$ is expressed in terms of σ_n, σ_m, and σ_e, being the average normal stress, the Von Mises effective stress and the mean stress, respectively, all remote from the cavity (recall that the stress state $\boldsymbol{\sigma}$ includes the cavity pressure). The normal stress σ_n is defined as $\sigma_n = (\mathbf{n}\cdot\boldsymbol{\sigma}\cdot\mathbf{n})$ where $\mathbf{n}$ is the unit normal vector on the grain boundary facet. The mean stress is given by $\sigma_m = \frac{1}{3}(\boldsymbol{\sigma}:\mathbf{I})$ and the effective stress σ_e is defined through the stress deviator $\mathbf{s} = \boldsymbol{\sigma} - \sigma_m\mathbf{I}$ as $\sigma_e = \sqrt{\frac{3}{2}\mathbf{s}:\mathbf{s}}$. Sintering stresses are neglected in this study.

The cavity growth rate by grain boundary diffusion, as determined originally by Hull and Rimmer [14], later improved (among other authors) by Needleman and Rice [12] and Sham and Needleman [13], is given by

$$\dot{V}_{diff} = 4\pi\mathscr{D}\frac{\sigma_n}{\ln(1/f) - \frac{1}{2}(3-f)(1-f)}. \tag{1}$$

Here the grain boundary diffusion parameter $\mathscr{D}$ is defined by $\mathscr{D} = D_B\delta_B\Omega/k\Theta$, where $D_B\delta_B$ is the boundary diffusivity, Ω is the atomic volume, and $k\Theta$ the energy per atom measure. The parameter f in equation (1) depends on the diffusive path length L_{diff} and the cavity radius a by

$$f = \left(\frac{a}{L_{diff}}\right)^2. \tag{2}$$

If the creep rates of the grain are negligible compared to the diffusional rate, as assumed in Ref. [14], the diffusive path length is equal to the half cavity spacing b. However, when creep deformations in the vicinity of the cavity become significant, the diffusive path length can be shortened, so as to accelerate the diffusive cavity growth [12, 13]; this will be specified later.

The cavity can also grow by creep of the adjacent grain material, which is here described by the power-law relation, where the effective creep strain rate, $\dot{\varepsilon}_e^c$ is given by

$$\dot{\varepsilon}_e^c = \dot{\varepsilon}_0\left(\frac{\sigma_e}{\sigma_0}\right)^n. \tag{3}$$

Here, σ_0 is a reference stress parameter, $\dot{\varepsilon}_0$ is a reference strain rate parameter, and n is the creep exponent. For cavity growth by creep under HA conditions, there are two modes [6]. The first mode is active when the cavities are so small that interactions between neighbouring cavities are negligible. When the porosity level a/b attains a certain value where interaction does take place, the other creep mode takes over. The porosity at which the modes change depends sensitively on the remote stress triaxiality σ_m/σ_e. Roughly speaking, the change of mode at low stress triaxialities is at larger a/b than at high triaxialities. In the first creep mode, the volumetric growth $\dot{V}_{cr}^L$ is given by

$$\dot{V}_{cr}^L = 2\pi\dot{\varepsilon}_m a^3 h(\psi)\ \mathrm{sign}(\sigma_m) r \tag{4}$$

$$\text{where}\begin{cases} r = \left[\alpha_n + \beta_n\left|\dfrac{\sigma_e}{\sigma_m}\right|\right]^n & \text{if } |\sigma_m/\sigma_e| \geq 1 \\ r = [\alpha_n + \beta_n]^n\left|\dfrac{\sigma_e}{\sigma_m}\right|^{n-1} & \text{if } |\sigma_m/\sigma_e| < 1 \end{cases} \tag{5}$$

and 'sign' denotes the sign of its argument. Here $\dot{\varepsilon}_m$ is a short hand notation introduced by

$$\dot{\varepsilon}_m = \dot{\varepsilon}_0\left|\frac{\sigma_m}{\sigma_0}\right|^n. \tag{6}$$

The parameters α_n and β_n depend on the creep exponent n and are defined by $\alpha_n = 3/(2n)$ and $\beta_n = (n-1)(n+0.4319)/n^2$. The high-triaxiality part of expression (5) is derived by Budiansky *et al.* [15]; the complementary part is introduced by Tvergaard in Ref. [8]. The relation is based on the growth of a cavity in an infinite creeping solid, so that cavity interactions are excluded.

In the second creep mode, the volumetric growth rate $\dot{V}_{cr}^{H}$ is given by

$$\dot{V}_{cr}^{H} = 2\pi\dot{\varepsilon}_m a^3 h(\psi)\,\mathrm{sign}(\sigma_m)\left[\frac{1}{1-(0.87a/b)^{3/n}}\right]^n s \quad (7)$$

$$\text{where}\begin{cases} s=\left(\alpha_n+\dfrac{1}{n}\dfrac{\mathrm{sign}(\sigma_n-\sigma_m)}{\mathrm{sign}(\sigma_m)}\left|\dfrac{\sigma_e}{\sigma_m}\right|\right)^n & \text{if } |\sigma_m/\sigma_e|\geq 1 \\ s=\left(\alpha_n+\dfrac{1}{n}\dfrac{\mathrm{sign}(\sigma_n-\sigma_m)}{\mathrm{sign}(\sigma_m)}\right)^n\left|\dfrac{\sigma_e}{\sigma_m}\right|^{n-1} & \text{if } |\sigma_m/\sigma_e|<1. \end{cases} \quad (8)$$

This relation, introduced in Ref. [6], is based on the cavity growth in an infinitely long creeping cylinder with radius b. The interaction between cavities is expressed in equation (7) through the cavity half spacing b.

The dependence of the diffusive cavity growth on the parameter f on the creep mode is expressed by:

$$\dot{V}_{diff}^{L} = \dot{V}_{diff}(f),\ f = \max\left[\left(\frac{a}{b}\right)^2, \left(\frac{a}{a+1.5L}\right)^2\right];$$

$$\dot{V}_{diff}^{H} = \dot{V}_{diff}(f),\ f = \left(\frac{a}{b}\right)^2, \quad (9)$$

where the stress and temperature dependent material parameter L is $L = (\mathscr{D}\sigma_e/\dot{\varepsilon}_e)^{1/3}$ $(\sigma_e \neq 0)$, first introduced by Needleman and Rice [12]. In the second creep mode, there is hardly any interaction between creep and grain boundary diffusion. Finally, the volumetric growth rate of the cavity is

$$\dot{V} = \max[\dot{V}_{cr}^{L} + \dot{V}_{diff}^{L},\ \dot{V}_{cr}^{H} + \dot{V}_{diff}^{H}]. \quad (10)$$

The spherical-caps shape of the cavity is maintained by rapid surface diffusion throughout the process, according to observations for 2.25Cr–1Mo steels in Ref. [11]. Then from the volumetric rate of change, the growth rate of the cavity radius is found as

$$\dot{a} = \dot{V}/(4\pi a^2 h(\psi)).$$

When $a/b = 1$ in the model (see Fig. 1), the cavities coalesce. However, analogous to observation of creep rupture [16], failure will occur earlier due to tearing of the ligament. It is assumed here that coalescence takes place when $a/b = 0.7$.

3. HA IN POLYCRYSTALLINE AGGREGATES

The investigating of HA on the second, grain-size length scale, allows one to analyze the interaction between the grain boundary cavitation and deformations of the adjacent grains. The initial carbide distribution is assumed to be uniform through the polycrystalline material. Since carbides are located at all grain boundaries, hydrogen attack in unstressed samples will result in cavitation at all facets. In cases where deviatoric stresses are applied on the sample, cavitation perpendicular to the maximum principle tensile stress can develop relatively faster. However, cavitation on the other facets can still occur because of the cavity gas pressure. In cases where the rate of change of cavitation is distributed nonuniformly, internal stresses tend to develop that constrain the evolution of relatively fast cavitating regions [7]. To analyze this interaction in some detail, the polycrystal model of Van der Giessen and Tvergaard [17, 18] is employed. This model was developed to investigate intergranular creep fracture, which is closely related to HA. The polycrystal HA model is described briefly; we refer to Ref. [18] for more details.

The two-dimensional (2-D) polycrystal model consists of an aggregate of regular hexagonal grains. In the undeformed state the grain boundary facet length is $2R_1$. In the present analyses, the unit cell depicted in Fig. 3 is used. The aggregate is subjected to macroscopic principal stresses Σ_1' and Σ_2' in the x^1- and x^2-directions, respectively, under plane strain conditions. In view of the symmetry requirements, these applied stresses are imposed by prescribing uniform velocities, such that Σ_1' and Σ_2' retain constant values.

Because all carbides are assumed to be identical, the cavities have the same internal cavity pressure p_m. Then (neglecting elastic volume changes) the cavity growth problem on grain-size length scale can be reformulated by exploiting the insensitivity of the creep and diffusion process on hydrostatic stress, as

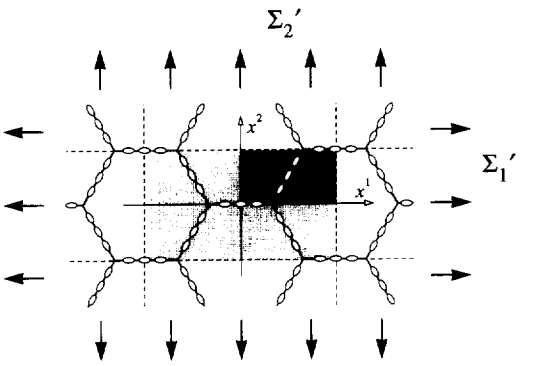

Fig. 3. Planar polycrystalline aggregate with the unit cell indicated by the light grey shading. Cavity growth is driven by the internal cavity pressure p_m and can be accelerated by macroscopic applied stresses Σ_1' and Σ_2'. Because of symmetries, only a quarter of the unit cell (the dark gray shaded area) has to be analyzed.

demonstrated above for the single cavity model. The hydrostatic stress p of the magnitude of the internal cavity pressure p_m is superposed on the polycrystal unit cell (instead of the single cavity unit cell in Fig. 2). This results in traction free cavity surfaces and average boundary stresses of $\Sigma_1' + p_m$, $\Sigma_2' + p_m$. For convenience, we say that the polycrystal is subjected to a biaxial stress state S, T with $S = \Sigma_2' + p_m$ and $T = \Sigma_1' + p_m$.

In the polycrystal model, the grains can deform elastically as well as by dislocation creep in an isotropic manner. Allowing for finite strains, the elastic stress–strain relationship $\mathring{\boldsymbol{\sigma}} = \mathscr{R}\mathbf{d}^e$ is written in terms of the Jaumann stress rate $\mathring{\boldsymbol{\sigma}}$ and the elastic strain rate $\mathbf{d}^e$. This elastic strain rate is the difference between the total strain rate $\mathbf{d}$ and the creep strain rates $\mathbf{d}^c$, so that the constitutive relations for the grain material can be written as

$$\mathring{\sigma}z = \mathscr{R}:(\mathbf{d} - \mathbf{d}^c)$$

with the creep strain rate $\mathbf{d}^c$ being given by

$$\mathbf{d}^c = \dot{\varepsilon}_e^c \frac{3\,\mathbf{s}}{2\sigma_e}.$$

In the case of creep, it has often been found that grains can slide relative to each other [19]. However, in the presence of the numerous grain boundary carbides, many carbides act as obstacles for sliding. Therefore grain boundary sliding is not assumed to take place in the polycrystal model for HA here.

The growing cavities on the grain boundary facet cause the adjacent grains to separate. The average separation is given by $\delta = V/(\pi b^2)$. Differentiation with respect to time gives the separation rate, also called the cavitation rate,

$$\dot{\delta} = \frac{\dot{V}}{\pi b^2} - \frac{2V\dot{b}}{\pi b^2 b}. \tag{11}$$

Due to a nonuniform stress state over the polycrystal aggregate and variations in cavitation state along the grain boundary, the separation rate can vary along the grain boundaries.

The numerical method used to solve the problem discussed above is largely similar to that in Refs [17, 18]. The grains themselves are discretized by quadrilateral Finite Elements (FE), each one of which consists of four triangular constant strain elements in a "crossed triangle" configuration. The FE grid used is depicted in Fig. 4. The HA and resulting grain boundary cavitation process is incorporated through grain boundary elements. In this case, the only deformation mode for these interface-type elements is the grain separation δ. Consistent with the FE representation inside the grains, the grain boundary elements use linear interpolations for δ and for the other grain boundary characteristics, such as cavity size a and half spacing b.

The governing equations for the grains as well as for the grain boundaries are solved in a linear incremental manner. The remote normal stress σ_n, to be used in the cavity growth relations (1)–(10), is taken from the grain boundary stress. The remote effective and mean stresses, σ_e and σ_m, are evaluated as averages from the corresponding stresses in the grain elements adjacent to the grain boundary. To increase the numerical stability of the procedure, a forward gradient approach is used to integrate the constitutive relations.

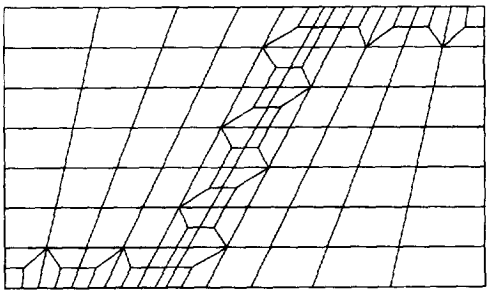

Fig. 4. Finite Element mesh of the quarter unit cell. The special grain boundary elements cannot be seen in the initial mesh geometry.

In the polycrystal HA model, the time to first coalescence is taken as the failure time of the polycrystal—although the aggregate can still transmit stress. It is likely that when some cavities have coalesced, macroscopic failure is at hand. Another reason to stop the analyses at first coalescence is that it is not clear what to take as the gas pressure acting on the microcracked surface.

4. TWO-DIMENSIONAL CONTINUUM DAMAGE RELATION

In this section, an analytical continuum damage relation (CDR) for HA is proposed, to be used in component-size analysis. In addition to the creep deformations of the grains, the relation must capture basically two different cavitation modes, as observed in Ref. [7]. It has ben shown in Ref. [7] that which of the two modes is active, is determined by the ratio of the separation rate due to cavitation and the creep rate of the grain, $\dot{\delta}/(R\dot{\varepsilon}_g)$. Here, $\dot{\delta}$ can be identified with the cavitation rate in the middle of a facet transverse to the macroscopic principal stress, and the creep deformability of the grain can be identified with the macroscopic effective creep strain rate $\dot{E}_e^c$, defined similar to equation (3) in terms of the macroscopic effective stress Σ_e, i.e. $\dot{E}_e^c = \dot{\varepsilon}_0(\Sigma_e/\sigma_0)^n$. In one extreme, where $\dot{\delta}/(R\dot{\varepsilon}_g)$ is large, the cavitation rates are much larger than creep deformations of the grain, and the grains will act as virtually rigid. This cavitation mode results in a uniform cavitation rate distribution, hence macroscopic dilatation. In the opposite extreme, when $\dot{\delta}/(R\dot{\varepsilon}_g)$ is small, the creep deformations of the grains get significant and cavitation will occur mainly on the facets perpendicular to the maximum principal macroscopic stress; this is the other cavitation mode.

The part of the CDR which encompasses the latter cavitation mode (when grains deform significantly by creep) is based on Tvergaard's constitutive relation for creeping polycrystals with grain boundary cavitation [8, 9], which is an extension of the analysis of diffusive cavitation by Rice [10]. The separation rate is taken from the opening rate $\dot{\delta}_{cr}$ of a virtual plane strain crack in an infinite creeping solid that is normal to the maximal principal tensile stress. This virtual crack is not traction free, but represents a cavitating grain boundary facet that transmits some normal stress σ_n. This stress is, in general, different from the maximal principal stress, i.e. the resolved normal stress S on the facet, determined from the stress state Σ and the unit facet direction tensor $\mathbf{m}$ as $S = \boldsymbol{\Sigma}:\mathbf{m}$ (for example, the components of $\mathbf{m}$ are $m_{ij} = \delta_{i2}\delta_{j2}$ when the x_2-direction is the direction of the macroscopic principal stress S as in Fig. 3). Based on the results of He and Hutchinson [20] for a traction-free crack in a plane strain creeping solid, but modified for the fact that the facet transmits a normal stress σ_n like in Ref. [9], the opening rate $\dot{\delta}_{cr}$ is given by

$$\dot{\delta}_{cr} = \frac{3\pi}{8}\sqrt{n}\frac{S-\sigma_n}{\Sigma_e}\dot{E}_e 2R.$$

The transmitted normal stress σ_n also drives the cavitation rate $\dot{\delta}$ through the cavity growth relations (1)–(11). The magnitude of the normal stress σ_n is now determined by requiring at any instant that $\dot{\delta}_{cr}(\sigma_n) = \dot{\delta}(\sigma_n)$. The value of the normal stress for which the equation holds will be denoted as $\sigma_{n,cr}$ and the associated separation rate as $\dot{\delta}_{cr}$. In view of this model, this part of the CDR will be referred to as the "plane strain crack mode".

The other part of the CDR describes the cavitation when the grains are virtually rigid. In this mode, the separation rate distribution $\dot{\delta}$ is uniform along the facet. Moreover, because of the rigidity of the grains in combination with the absence of grain boundary sliding, the cavitation on adjacent grain boundaries is geometrically coupled [7], so that the separation rates on adjacent grain boundaries are equal in the case of regular hexagonal grains. Note that this requires the development of internal stresses on the grain-size scale [7]. The uniform separation rate distribution results in a macroscopic (2-D) dilatational strain rate $\dot{E}_m$, as is illustrated in Fig. 5. The stress component conjugate to this macroscopic dilatation rate is the macroscopic hydrostatic stress Σ_m. Hence, the normal stress on the facets in the rigid grain cavitation mode is $\sigma_{n,rg} = \Sigma_m$, with $\Sigma_m = (S+T)/2$ for plane strain. The associated separation rate is denoted as $\dot{\delta}_{rg}$.

The cavitation rate $\dot{\delta}$ depends not only on the particular σ_n, but also on the effective and mean stresses in the neighbourhood of the facet, through the cavity growth rate $\dot{V} = \dot{V}(\sigma_n, \sigma_e, \sigma_m)$ and the local creep rate [see equation (11)]. In order to ensure compatibity of creep deformations in the neighbourhood of grain boundaries with the macroscopic creep rates, the local stress deviator $\mathbf{s}$ is taken to be equal to the macroscopic stress deviator $\mathbf{S}$. Hence, the effective stress at the grain boundary is $\sigma_e = \Sigma_e$; but evidently, $\sigma_m \neq \Sigma_m$. The local mean stress can be found by noting from the definition $\mathbf{s} = \boldsymbol{\sigma} - \sigma_m\mathbf{I}$ that $\sigma_m = (\boldsymbol{\sigma} - \mathbf{s}):\mathbf{m}$ so that with $\mathbf{s} = \mathbf{S}$ and with $\sigma_n = \boldsymbol{\sigma}:\mathbf{m}$ we have $\sigma_m = \sigma_n - \mathbf{S}:\mathbf{m}$. For plane strain under principal stresses S and T, this reduces to $\sigma_m = \sigma_n - (S-T)/2$.

Now, for the two modes we can compute the respective cavitation rates. The selection of which of the two modes is active in the CDR is proposed here to be determined by the maximum of both cavitation rates: $\dot{\delta} = max[\dot{\delta}_{cr}, \dot{\delta}_{rg}]$.

Because of the fact that the magnitude of $\dot{\delta}$ depends on e.g. the cavitation state a/b, and that stress redistributions over the polycrystal aggregate occur during the lifetime, the ratio $\dot{\delta}/(R\dot{\varepsilon}_g)$ varies during damage evolution. In the case of a stationary uniaxial applied stress, one can in fact show that the ratio increases monotonically during damage evolution. Then, in the beginning of the lifetime the cavitation is in accordance with the plane strain crack mode, whilst it is possible that cavitation at the end of the lifetime occurs in the rigid grain mode.

Once the cavitation mode is established, the associated (macroscopic) strain rates $\mathbf{D}^c$ can be determined. In the case of the plane strain crack mode, we have

$$\mathbf{D}^c_{cr} = \dot{\varepsilon}_0\left(\frac{\Sigma_e}{\sigma_0}\right)^n\left[\frac{3}{2}\frac{\mathbf{S}}{\Sigma_e} + \rho\left\{\frac{3n-1}{2n+1}\frac{\mathbf{S}}{\Sigma_e}\left(\frac{S-\sigma_n}{\Sigma_e}\right)^2 + \frac{2}{n+1}\frac{S-\sigma_n}{\Sigma_e}\mathbf{m}\right\}\right], \quad (12)$$

based on He and Hutchinson [20] and Hutchinson [21], and similar to Ref. [9]. The parameter ρ reflects the cavitating facet (or crack) density expressed in $\rho = 3\pi/8R^2N(n+1)\sqrt{n}$, where N is the number of cavitating facets per unit area. As it is assumed that all transverse facets will cavitate, N is given by

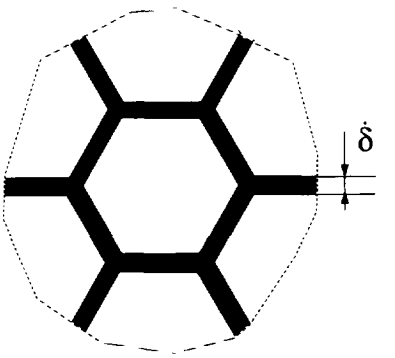

Fig. 5. In the rigid grain cavitation mode, a virtually uniform distribution of the rate of cavitation along the grain boundaries results in a macroscopic dilatation.

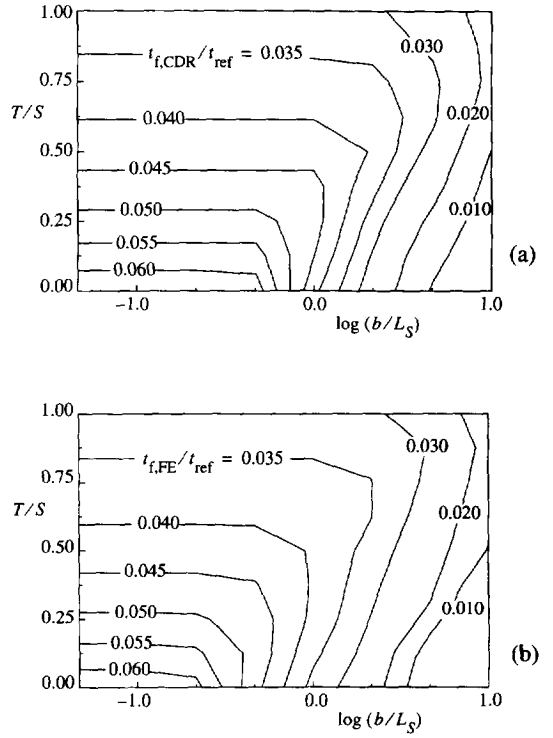

Fig. 6. Contours of time to failure as a function of triaxiality T/S and of log (b/L_S) according to (a) the CDR and (b) the unit cell FE analysis.

$N = 1/A_{gr}$ with A_{gr} the average grain area. For the polycrystal shown in Fig. 3, which is built up by regular hexagonal grains with initial facet length $2R_I$, we have $N = 1/(6\sqrt{3}R_I^2)$.

In the case of cavitation according the rigid grain mode, the inelastic strain rates are given by

$$\mathbf{D}^c_{rg} = \dot{\varepsilon}_0\left(\frac{\Sigma_e}{\sigma_0}\right)^n \frac{3}{2}\frac{\mathbf{S}}{\Sigma_e} + \Omega\frac{\dot{\delta}_{rg}}{R_I}\mathbf{I}^* \qquad (13)$$

where the first term, like in equation (12), reflects the creep deformations of the grain, and the second term the uniform cavitation which results in a 2-D hydrostatic dilation. The geometrical parameter Ω is $\Omega = 1/(2\sqrt{3})$ in the case of 2-D regular hexagonal grains, assuming that the strains remained small, thus $R_I \approx R$, and that $\delta_{rg} \ll R_I$. The tensor $\mathbf{I}^*$ is a special unit tensor which satisfies the plane strain condition, $I^*_{33} = 0$.

5. VERIFICATION OF THE 2-D CDR

To answer the question of how accurate the proposed CDR is, the failure times (i.e. time to first cavity coalescence) determined with the CDR are compared with the detailed FE analyses of the polycrystal HA model. The assumed initial cavitation along the grain boundaries is characterized by $(a/b)_I = 0.1$ and $(b/R)_I = 0.1$. The cavity equilibrium cavity tip angle ψ is taken as $\psi = 75°$. The diffusion and creep parameters are characterized by the

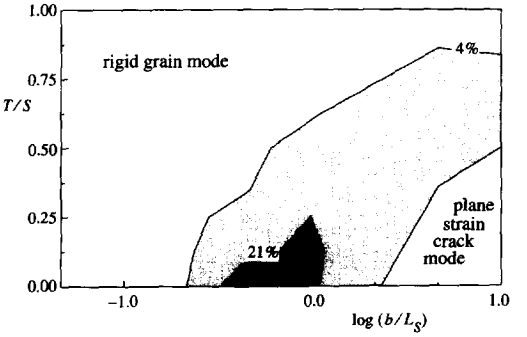

Fig. 7. Illustration of the accuracy of the CDR by plotting the deviation $(t_{f,CDR} - t_{f,FE})/t_{f,FE}$ of the CDR results from the unit cell FE analyses as shown in Fig. 6.

dimensionless parameter b_I/L_S, where L_S is defined as $L_S^3 = (\mathscr{D}S)/\dot{\varepsilon}^c_S$, with $\dot{\varepsilon}^c_S = \dot{\varepsilon}_0(S/\sigma_0)^n$. The creep exponent n is taken to be $n = 5$. For comparison, this parameter ranges from $\log(b_I/L_S) = -1.33$ where cavitation is diffusion dominated and the grains act virtually as rigid, via $\log(b_I/L_S) = 0$ where cavitation is creep constrained, till $\log(b_I/L_S) = 1$ where even cavitation can be creep controlled. The regime is scanned with a step size of $\log(b_I/(\Delta L_S)) = 1/3$. The macroscopic stress state S,T (recalling that $S = \Sigma'_2 + p_m$ and $T = \Sigma'_1 + p_m$) ranges from the situation where high internal cavity pressure dominates the stress situation (e.g. in practical cases of very aggressive carbides), represented by $T/S \approx 1$, till the situation where uniaxial macroscopic applied stress dominates (e.g. when the carbides can be classified as very stable) represented by $T/S \approx 0$. The range is scanned with a step size of $(\Delta T)/S = 1/8$. To ensure that elastic deformations can be disregarded, the Young's modulus E is specified as $S/E = 1.0 \times 10^{-5}$. The results are presented in a dimensionless way by introducing a reference time scale $t_{ref} = b_I^3/(\mathscr{D}S)$, based on diffusive cavitation.

Figure 6(a) presents the time to failure $t_{f,CDR}$ determined with the CDR as a function of the stress triaxiality T/S and the stress dependent material parameter b_I/L_S. Comparing Fig. 6(a) with Fig. 6(b), which depicts the times to failure in the unit cell

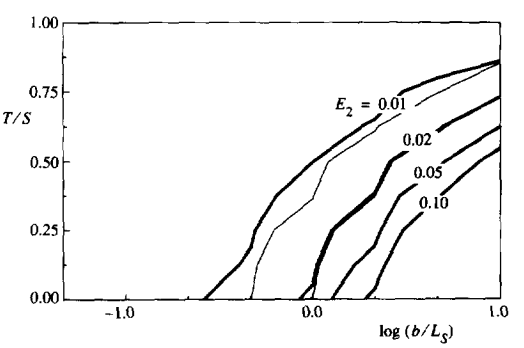

Fig. 8. Comparison of the macroscopic strain E_2 at failure as predicted by CDR (thick lines) and by the unit cell FE analyses (thin lines).

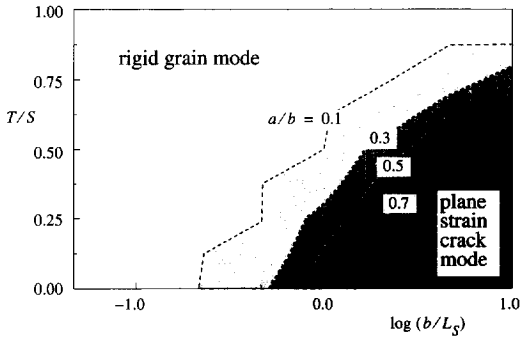

Fig. 9. The ratio a/b at which transition of cavitation mode takes place in the CDR from the plane strain crack mode to the rigid grain mode.

analyses, $t_{f,FE}$, both figures show a reasonable similarity in shape of the isofailure lines. To assess more precisely how accurate the CDR is, the deviation is plotted in Fig. 7. As can be seen in the figure, in most cases the deviation between the CDR and unit cell result is smaller than a few percent. The maximum deviation found is 35% at log $(b_l/L_S) = -0.33$ and $T/S = 0$. A similarly good agreement is seen in Fig. 8 for the macroscopic strain E_2 at failure.

The predictions with the CDR have their largest deviation from the unit cell analyses in the situations where a transition of the cavitation mode takes place. In the cases here, the transition is always from the plane strain crack mode into the rigid grain mode, as can be seen in Fig. 9 showing the a/b when transition occurs. Because both models are based on extreme situations, it is understandable that in intermediate cases the predicted cavitation rates by the CDR are not very accurate. However, the total error introduced should remain limited because the transition regime is restricted as a consequence of the continuous increase of the mode determining parameter $\dot{\delta}/(R\dot{\varepsilon}_g)$ (where $\dot{\delta}$ increases with a/b under a constant stress state).

To assess the error introduced during transition of cavitation mode, we plot the cavitation and normal stress evolution in the centre of the transverse facet for three different cases, classified by log $(b_l/L_S) = -1.00$, -0.33, 0.33 and $T/S = 0$. In Fig. 10(a) where log $(b_l/L_S) = -1.00$, the cavitation evolution in the rigid grain mode in the CDR agrees well with the results obtained in the unit cell analysis. Also the normal stresses found in the unit cell model, plotted in Fig. 10(d), are seen to agree well with the normal stress of the rigid grain mode in which, for this case, $\sigma_n = S/2(= \Sigma_m)$. In the opposite cavitation mode where log $(b_l/L_S) = 0.33$, the problem is creep dominated and cavitation has hardly any influence on the strain rates. This situation is picked up well by the plane strain crack mode of the CDR as can be seen in Fig. 10(c). Also the normal stress for the plane strain crack mode of the CDR agrees rather well with the cell model normal stress, as can be seen in Fig. 10(f). So in both extreme cases, the cavitation and the normal stress are captured well by the CDR. Only in the intermediate situation is the CDR less

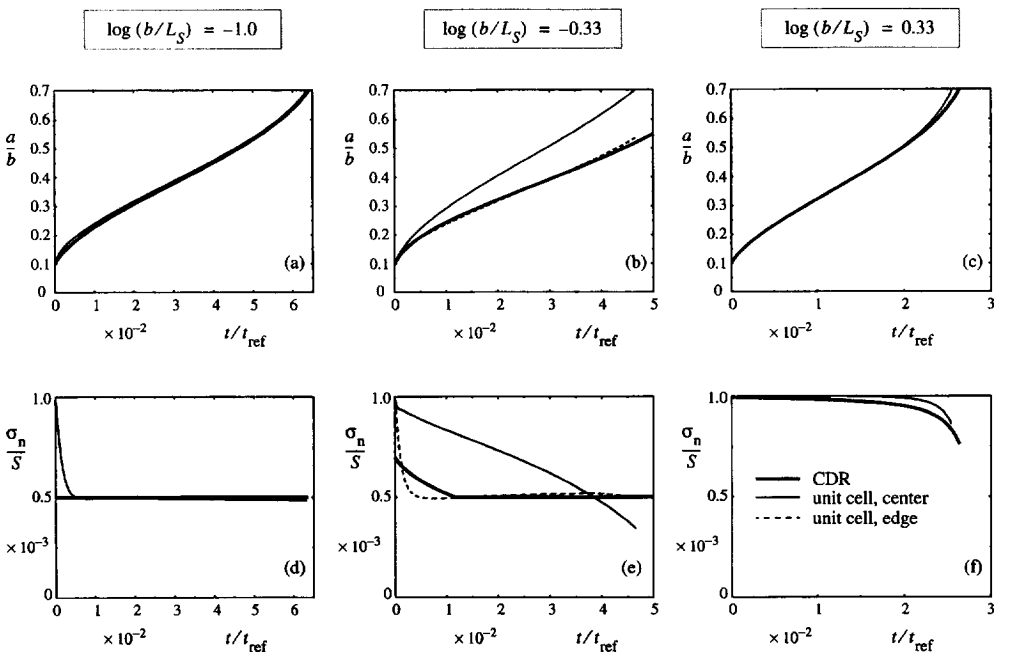

Fig. 10. Cavity evolution, expressed in a/b, [(a), (b), (c)] and normal stress development [(d), (e), (f)] under uniaxial macroscopic stress $T/S = 0$ for three different material parameters. In (a) and (d)log $(b_l/L_S) = -1.00$; in (b) and (e) log $(b_l/L_S) = -0.33$; in (c) and (f) log $(b_l/L_S) = 0.33$. The CDR results are the thick solid lines, the thin solid lines the unit cell FE results in the centre of the transverse facet. In (b) and (e) the dashed lines are results close to the edge of the transverse facet.

accurate, as can be seen in Figs 10(b) and (e). Here, in addition to results at the facet centre, the situation close to the edge of the transverse facet is depicted, thus showing that the behaviour is rather nonuniform over the facet. It is observed that the CDR predictions agree much better with the cavitation and normal stress development near the edge of the facet than at the centre. The normal stress development according to the CDR at the first stages gives an average representation of the distribution over the facet in the cell analyses, but after some time it settles at a value of $\sigma_n = \Sigma_m$ as also found near the facet edge. Hence, in those latter stages, cavitation is taken to be according to the rigid grain mode in the CDR predictions.

Finally, it should be noted that if the inclined facet could not cavitate at all, the normal stress drops much further, as in the case of creep constrained cavitation in creep rupture [22, 18]. The subsequent times to failure would be completely different.

6. THREE-DIMENSIONAL GENERALIZATION

Since the CDR relation presented and validated above is based on two analytical models, a straightforward generalization can be made into a 3-D version of the CDR. Instead of (2-D) hexagons, the grains are now taken as (3-D) regular truncated octahedra (see Fig. 11). The virtual facet crack is modelled as a penny shaped crack.

In the now called "penny shaped crack mode", the cavitation rate is determined by demanding that the cavitation rate is equal to the crack opening rate of the penny shaped crack $\dot{\delta}_p$, $\dot{\delta}(\sigma_n) = \dot{\delta}_p(\sigma_n)$, as in the procedure for 2-D giving the facet normal stress σ_n. The crack opening rate for a penny shaped crack $\dot{\delta}_p$ is given by He and Hutchinson [20] as

$$\dot{\delta}_p = \frac{4}{\pi}\left(1 + \frac{3}{n}\right)^{-1/2} \frac{S - \sigma_n}{\Sigma_e} \dot{E}_e^c 2R, \quad \dot{E}_e^c = \dot{\varepsilon}_0 \left(\frac{\Sigma_e}{\sigma_0}\right)^n.$$

It is noted that in evaluating the cavitation rate $\dot{\delta}(\sigma_n, \sigma_e, \sigma_m)$ the value of σ_m is taken as $\sigma_m = \sigma_n - \mathbf{S}:\mathbf{m}$, while σ_e is chosen to be equal to Σ_e. The corresponding inelastic strain rate of the polycrystal material is then given by [cf. equation (12)]

$$\mathbf{D}_p^c = \dot{\varepsilon}_0 \left(\frac{\Sigma_e}{\sigma_0}\right)^n \left[\frac{3}{2}\frac{\mathbf{S}}{\Sigma_e} + \rho\left\{\frac{3n-1}{2n+1}\frac{\mathbf{S}}{\Sigma_e}\left(\frac{S-\sigma_n}{\Sigma_e}\right)^2 + \frac{2}{n+1}\frac{S-\sigma_n}{\Sigma_e}\mathbf{m}\right\}\right],$$

with $S = \boldsymbol{\Sigma}:\mathbf{m}$ being the maximum principal macroscopic stress normal to the facet with unit direction tensor $\mathbf{m}$, where $\boldsymbol{\Sigma}$ is the macroscopic stress tensor consisting of the applied stress $\boldsymbol{\Sigma}'$ and the cavity pressure p_m, $\boldsymbol{\Sigma} = \boldsymbol{\Sigma}' + p_m\mathbf{I}$. The parameter ρ, depending on the number of cavitating facets per unit volume, N, and the radius of the penny shaped crack R, is in 3-D given by $\rho = 4R^3N(n+1)\sqrt{(1+3/n)}$. Because all transverse grain boundaries cavitate, the number of facets per unit volume N is $N = 1/\bar{V}_{gr}$, where $\bar{V}_{gr}$ is the average volume of a grain. In the case of the regular truncated octahedra, the number of cavitating facets is $N = 0.042R_I^{-3}$, when the radius R_I is based on the average facet area of the truncated octahedron.

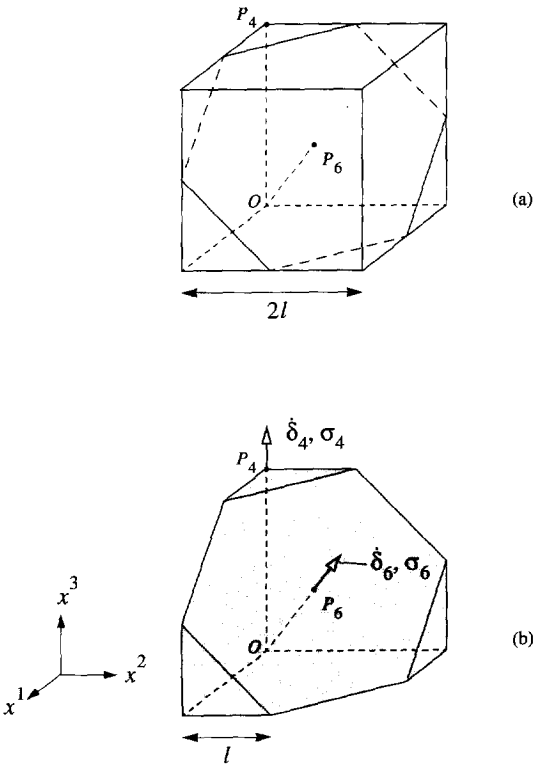

Fig. 11. (a) Elementary cube consisting of two times one-eigth of a truncated-octahedral grain, where the hexagon is their common grain boundary facet. Other (square) grain boundary facets are built up of four triangles. The 3-D polycrystal aggregate is constructed with this elementary cell, where each face of the cube is a plane of reflective symmetry in the aggregate. (b) Definition of quantities for one-eighth of a grain used in the derivation of the value of Ω in the Appendix.

In the rigid grain mode, the strain rate $\mathbf{D}_{rg}^c$ consists of a pure creep part and a dilatation part due to the isotropic cavitation [cf. equation (13)]

$$\mathbf{D}_{rg}^c = \dot{\varepsilon}_0 \left(\frac{\Sigma_e}{\sigma_0}\right)^n \frac{3}{2}\frac{\mathbf{S}}{\Sigma_e} + \Omega\frac{\dot{\delta}_{rg}}{R_I}\mathbf{I}, \tag{14}$$

where Ω is the geometrical parameter for the dilatation depending on the grain shape, and $\mathbf{I}$ is the (now standard) unit tensor. The value of the geometrical parameter Ω for grains having the truncated octahedral shape is derived in the Appendix and is found to be $\Omega = 0.31$. The cavitation rate $\dot{\delta}_{rg}$ resulting in hydrostatic dilatation is determined by the macroscopic mean stress, $\sigma_n = \Sigma_m$.

The criterion to decide which of the two deformation modes is active, reads:

$$\dot{\delta} = \max[\dot{\delta}_p, \dot{\delta}_{rg}]. \quad (15)$$

The macroscopic constitutive relations are finally completed by the elastic rate expression $\overset{\circ}{\boldsymbol{\Sigma}} = \mathscr{R}(\mathbf{D} - \mathbf{D}^c)$ where $\mathbf{D}^c$ is either $\mathbf{D}^c_p$ or $\mathbf{D}^c_{rg}$ depending on the outcome of the selection [15].

The accuracy of the 3-D CDR is unknown at this stage since an FE programme for verification on the basis of a 3-D polycrystalline model generalizing that in Fig. 3 is not yet available. However, the extreme cavitation modes are expected to be captured with reasonable accuracy. Similar as for 2-D, a significant error is only expected in the transition regime between the modes.

7. CONCLUSION

A macroscopic continuum damage relation (CDR) has been proposed to describe the grain boundary cavitation process of hydrogen attack (HA) at the macroscopic scale. The CDR is based on the creep deformations of the grains in combination with two possible grain boundary cavitation modes as extreme cases. In one mode, creep deformations of the grains are negligible, so that the cavitation rate is uniform along all grain boundaries thus resulting in a hydrostatic dilatation. In the other mode, creep deformations of the grains are significant and cavitation develops most rapidly on facets perpendicular to the macroscopic principal stress. The fastest cavitating mode is the mode active. The plane strain version of the CDR has been verified over a range of stress triaxialities and material properties against the numerical results of a much more detailed unit cell analysis of a planar polycrystalline aggregate. Finally, a generalization of the CDR to fully three-dimensional states is given.

The formulation of the CDR, as well as the verification of the plane strain version, presumes that the principal axes of macroscopic stress do not rotate during the process. Moreover, it is implicit in the development that the maximum principal stress component is always in the same direction. If this is not true, the facets that have optimal orientation for cavitation change during the process. Then, it does not suffice to consider a scalar representation of damage (in terms of a/b as in the present formulation, but one would need a tensorial characterization.

The CDR can be employed to study the HA process at the size scale of engineering components, like in vessels, notches or weldings. Aspects like, for example, the influence of gradients in temperature, stress or hydrogen pressure on the HA evolution can be studied. Preliminary results are reported in Ref. [23].

Acknowledgements—The research of Marc van der Burg is sponsored by Shell Research and Technology Centre, Amsterdam.

REFERENCES

1. *American Petroleum Institute Publication* **941,** 4th edition, April, 1990.
2. Parthasarathy, T. A., *Acta metall.*, 1985, **33,** 1673.
3. Shewmon, P. G. *Acta metall.*, 1987, **35,** 1317.
4. Van der Burg, M. W. D., Van der Giessen, E. and Brouwer, R. C., *Acta mater.*, 1996, **44,** 505.
5. Shih, H.-M. and Johnson, H. H., *Acta metall.*, 1982, **30,** 537.
6. Van der Giessen, E., Van der Burg, M. W. D., Needleman, A. and Tvergaard, V., *J. Mech. Phys. Solids*, 1995, **43,** 123.
7. Van der Burg, M. W. D. and Van der Giessen, E., *Mat. Sci. Eng. A*, 1996, **220,** 200.
8. Tvergaard, V., *J. Mech. Phys. Solids*, 1984, **32,** 373.
9. Tvergaard, V., *Acta metall.*, 1984, **32,** 1977.
10. Rice, J. R., *Acta metall.*, 1981, **29,** 675.
11. Shewmon, P. G., *Mat. Sci. Tech.*, 1985, **1,** 1.
12. Needleman, A. and Rice, J. R., *Acta metall.*, 1980, **28,** 1315.
13. Sham, T.-L. and Needleman, A., *Acta metall.*, 1983, **31,** 919.
14. Hull, D. and Rimmer, D. E., *Phil. Mag.*, 1959, **4,** 673.
15. Budiansky, B., Hutchinson, J. W. and Slutsky, S., in *Mechanics of Solids: The Rodney Hill 60th Anniversary Volume*, ed. H. G. Hopkins and M. J. Sewell. Pergamon Press, Oxford, 1982, p. 13.
16. Cocks, A. C. F. and Ashby, M. F., *Progress in Materials Science*, 1982, **27,** 199.
17. Van der Giessen, E. and Tvergaard, V., *Acta metall. mater.*, 1994, **42,** 959.
18. Van der Giessen, E. and Tvergaard, V., *Mech mater.*, 1994, **17,** 47.
19. Ashby, M. F., *Surface Sci.*, 1972, **31,** 498.
20. He, M. Y. and Hutchinson, J. W., *J. Appl. Mech.*, 1981, **48,** 830.
21. Hutchinson, J. W., *Acta metall.* , 1983, **7,** 1079.
22. Dyson, B. F., *Metal Science*, 1976, **10,** 349.
23. Van der Burg, M. W. D., Van der Giessen, E. and Tvergaard, V., in *Localized Damage IV: Computer-Aided Assessment and Control*, ed. H. Nisitani *et al.* Computational Mechanics Publications, Southampton, 1996, p. 641.
24. Anderson, P. M. and Rice, J. R., *Acta metall.*, 1985, **33,** 409.

APPENDIX

In this Appendix we derive the value of the geometrical parameter Ω to be used in equation (14) by considering 3-D grains which have the shape of truncated octahedra. This configuration has been used previously by Anderson and Rice [24] as a representative grain shape. A truncated octahedron can be regarded as the Voronoi cell of the body-centred cubic lattice, and consists of six square facets and eight hexagonal facets (see Fig. 11). With $2l$ denoting the size of the elementary cell shown in Fig. 11(a) and taking Cartesian axes (x^1, x^2, x^3) with origin O at the centroid of the truncated octahedron, the centre P_4 of one of the square facets is at $(0, 0, 2)\ l$ and the centre P_6 of one of the hexagonal facets is at $(1, 1, 1)\ l$. The areas of the two families of facets are $A_4 = 2l^2$ and $A_6 = 3\sqrt{3}l^2$.

On each of the square facets as well as on each of the hexagonal facets we assume uniform cavitation, corresponding to instantaneous separation rates $\dot{\delta}_4$ and $\dot{\delta}_6$, respectively. In the rigid grain mode of cavitation, the $\dot{\delta}_4$s and $\dot{\delta}_6$s are the same for all square and hexagonal facets, respectively, and are kinematically coupled along their intersections in order that the resulting overall strain rate $\dot{\mathbf{E}}$ is a pure dilation, i.e. $\mathbf{D} = \dot{E}_m\mathbf{I}$. Now, the separation rate on the square facets give

a dilatation rate of $\frac{1}{2}\dot{\delta}_4/(2l)$, while those on the hexagonal facets give $\frac{1}{2}\dot{\delta}_6/(\sqrt{3}l)$; requiring those two to be equal to $\dot{E}_m$ yields

$$\dot{E}_m l = \frac{\dot{\delta}_4}{4} = \frac{\dot{\delta}_6}{2\sqrt{3}} \tag{A1}$$

(as opposed to this result, note that in the 2-D model with hexagonal grains, the ratio of the separation rates on all facets is exactly unity, as illustrated in Fig. 5).

Now, the stresses that are energetically conjugate to the separation rates are the stresses normal to the facets. Denoting the average normal stresses on the square and hexagonal facets by σ_4 and σ_6, respectively, the virtual rate of work $\dot{W}_i$ on the facets due to the uniform separation, and measured per unit volume of the elementary cell [Fig. 11(b)], is given by

$$\dot{W}_i = 6\left(\frac{A_4}{4}\sigma_4\frac{\dot{\delta}_4}{2}\right) + A_6\sigma_6\dot{\delta}_6,$$

when, from now on, all rates are interpreted as virtual changes. On the other hand, the virtual work $\dot{W}_e$ (per unit volume of the elementary cell) of the macroscopic stresses $\boldsymbol{\Sigma}$ associated with the associated macroscopic dilatation $\mathbf{D}$ is

$$\dot{W}_e = (2l)^3\boldsymbol{\Sigma}:\mathbf{D} = (2l)^3 3\Sigma_m\dot{E}_m,$$

with $\Sigma_m = \frac{1}{3}\boldsymbol{\Sigma}:\mathbf{I}$ being the macroscopic mean stress. Since the macroscopic dilatation due to the separation rates of the facets is the only deformation mode in the rigid grain mode considered here, the principle of virtual work requires $\dot{W}_i = \dot{W}_e$ for all $\dot{\delta}_4$, $\dot{\delta}_6$, $\dot{E}$ satisfying (A1). This readily leads to the equilibrium condition

$$4\Sigma_m = \sigma_4 + 3\sigma_6. \tag{A2}$$

According to the proposed CDR expression (14) for the rigid grain mode, the dilatation $\dot{E}_m$ would be written as

$$\dot{E}_m = \Omega\frac{\dot{\delta}_{rg}}{R_l}, \tag{A3}$$

with $\dot{\delta}_{rg}$ being determined by the cavity growth relations (10) and (11) by substituting for σ_n the macroscopic hydrostatic stress Σ_m. This cannot be reconciled in general with the treatment above for the truncated octahedron, since we have found that the separation rates on different families of facets are different. Moreover, the separation rate $\dot{\delta}_4$ on the square facets would be determined by the corresponding average normal stress σ_4, and similarly for the hexagonal facets, while both normal stresses are in general different from Σ_m. However, it is possible to make the connection in an approximate manner by noting that in the rigid grain mode, cavity growth is dominated by diffusive growth and that in this case the separation rate depends linearly on the facet normal stress, $\dot{\delta}_4(\sigma_4)\propto\sigma_4$ and $\dot{\delta}_6(\sigma_6)\propto\sigma_6$. Then, by assuming that the normal facet stresses have the same ratio as the corresponding separation rates according to equation (A1), i.e.

$$\frac{\sigma_4}{4} = \frac{\sigma_6}{2\sqrt{3}},$$

we find from equation (A2) that $\sigma_4 = 8\Sigma_m/(2+3\sqrt{3})$, so that from equation (A1) we have

$$\dot{E}_m = \frac{\dot{\delta}_4(\sigma_4)}{4l} \approx \frac{2}{2+3\sqrt{3}}\frac{\dot{\delta}(\Sigma_m)}{l} \approx 0.31\,\frac{\dot{\delta}(\Sigma_m)}{R_l}. \tag{A4}$$

Here, we have used the substitution $l \approx 0.906R_l$ in terms of the average facet radius R_l. Thus, we conclude by comparing with equation (A3) that $\Omega \approx 0.31$ for truncated octahedral grains. Note that this is only slightly different from the value $\Omega = 1/(2\sqrt{3}) \approx 0.29$ for planar hexagonal grains.

It should be noticed, however, that the above derivation assumes that the pre-factors in $\dot{\delta}_4(\sigma_4)\propto\sigma_4$ and $\dot{\delta}_6(\sigma_6)\propto\sigma_6$, respectively, are a function of the amounts of damage on the respective facets, and that these are in general not identical (contrary to the situation in the planar model discussed earlier). Moreover, even if the amounts of damage are identical instantaneously, they will evolve differently since σ_4 and σ_6 are different. Hence, for 3-D grains as truncated octahedrons (and presumably also for other grain shapes), the expression (A4) is an approximation.